

CHAPTER 6. NUMERICAL TESTING OF AXIAL LOAD CAPACITY OF A DRILLED SHAFT WITH ANOMALIES

Various tests and analytical methods have been developed to evaluate the axial load capacity of a drilled shaft. Design requires proper sizing of the drilled shaft for sufficient axial load capacity. Static load tests are generally performed on full-scale prototype shafts to obtain load-settlement curves. Analytical methods, based on concrete, soil, and rock properties obtained from laboratory or in-situ tests, are used to determine the ultimate load capacity of a drilled shaft. This study focuses on axial load capacity and static load tests, to demonstrate the capabilities of a modeling approach to determine the effect of anomalies on capacity. Numerical modeling can also analyze dynamic and lateral loads, which may be the control factors in certain situations.

Drilled shafts transfer applied axial loads to the ground via two mechanisms: side friction and toe bearing. Since geo-materials are highly inhomogeneous, anisotropic, non-linear, and non-elastic, the quality of the drilled shaft and interaction of the shaft and surrounding soils are major factors to control performance of the foundation. In situ prototype tests provide reliable design parameters for shaft design, but can be expensive and time consuming for many applications. Analytical methods can provide economical alternatives for simulating field conditions. With numerical modeling, site specific geology and material properties obtained from field investigations can be reproduced, and the effects of various loading conditions for drilled shaft design criteria can be analyzed.

6.1 Axial Loading Model Analysis

Concerns have recently been raised that design procedures for drilled shafts prescribed by the American Association of State Highway and Transportation Officials (AASHTO) do not incorporate the effect of soil density or cementation, specifically for end bearing shafts. In this study, common soil and rock properties encountered in highway engineering, with corresponding boundary conditions, are incorporated into a model that is socketed in bedrock for an end bearing shaft. The same defect at two different depths in the shaft is introduced into the model, to compare performance under axial loading.

In the axial loading model analysis, the drilled shaft is installed inside four different geo-materials. The order of the materials from the top to the toe of the drilled shaft is dry sand, wet sand, clay, and bedrock. The depths of each material and their relative elevations are showed in Figure 6.1. The toe of the drilled shaft is socketed 0.5 m in bedrock. The geo-material properties of this model are specified the same as other modeling this study (see section 6.1 for the specifications). The bottom of the model is constrained from displacement in the vertical (Z) direction and the surrounding boundary conditions are constrained of displacements in horizontal (X - Y) directions but vertical displacement is allowed (i.e. compaction and settlement are allowed). The ground surrounding the drilled shaft model has been expanded from 1.5 m to 2 m on a side, to reduce boundary condition effects. Elements at the base of the model are static.

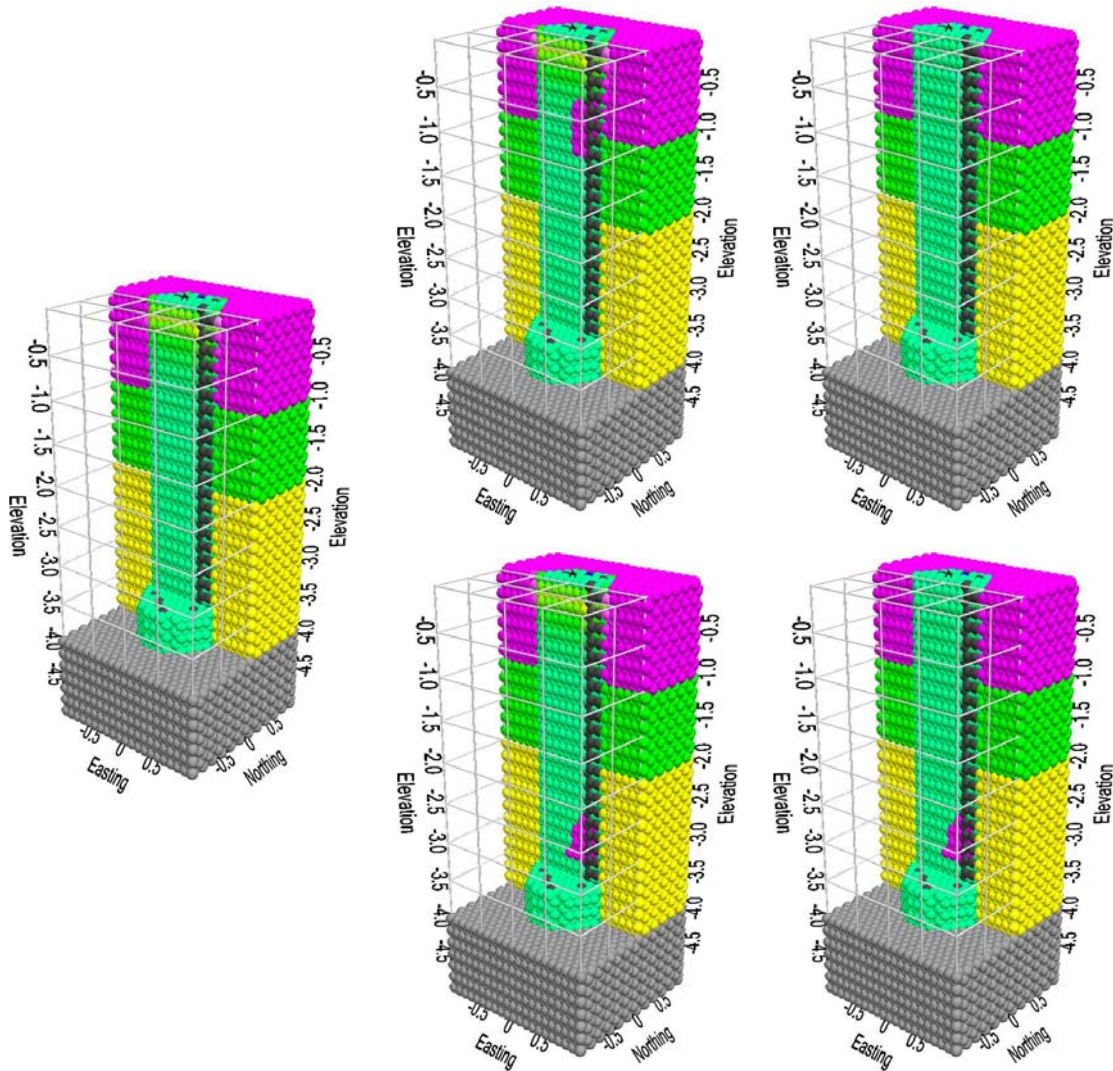


Figure 6.1. Plot. Compression Stress at Initial Vertical Displacement. Top: Sand Intrusion at 1 m Depth. Bottom: Sand Intrusion 3 m Depth. Left: Compression Stress, No Defect. Center: Compression Stress. Right: Compression Stress Difference

Axial loading is applied uniformly on the top of the drilled shaft by pushing the shaft slowly downward with uniform displacement (standard displacement control test). The vertical force component is calculated from summing spring compression over the constrained elements at the top of the shaft. Two small sized defects (20% reduction in velocity) are introduced into the drilled shaft at depth of 1 m and 3 m, by replacing drilled shaft material with dry sand for comparison to a drilled shaft with no defect. Compacted and loosened conditions are also simulated to compare the effect of the density or cementation of the soil. The modeling results at the different loading/displacement stages are plotted in figures and graphs. The observations are presented and discussed in the following sections.

6.1.1 Displacement of 4 mm

The stress intensity in the drilled shaft at an initial displacement of 4 mm, measured at the top of the shaft, is plotted in Figure 6.2. Three models showing stress intensity are plotted in the figure. The left plot is the stress of the shaft without a defect. The center top and bottom plots represent the stress of the shaft with a defect at a depth of 1 m and 3 m, respectively. The right plots show the stress differences between the non-defective and the defective shafts.

The center plots show highest stress in the top of the shaft, gradually decreasing with depth. The stress is insignificant after a depth of 0.5 m. The stress build-up in the top of the shaft is a result of the friction and interlocking between the concrete and the surrounding ground. As the shaft moves, the surrounding ground compresses, resisting a significant proportion of the load. The drilled shaft is not so much compressed between the surface and the bedrock as it is compressed between the surface and the surrounding ground. In this case, the shaft experiences the most compression between the surface and the top of the wet sand.

The difference plots on the right of the figure show no change in stress from the shaft with no defect. This indicates that the defect at both depths of the shaft has no influence on the compression stress at this displacement.

6.1.2 Displacement of 4 cm

The stress intensity at a displacement of 4 cm is plotted in Figure 6.3. This is at the stage when the shaft is usually considered to have failed due to the large displacement. As seen from the plot on the left (non-defective shaft) and the plots in the center (defective shaft), the compression stress is at very high levels in the top 0.75 m of the shaft. Regions in the shaft where the stress is red have high potential to fracture. The stress abruptly decreases in the next 0.25 m, and is insignificant after a depth of 1 m. The shaft still experiences the most compression between the surface and the top of the wet sand. The wet sand layer is able to sustain slightly more load than the dry sand layer, and is most likely the cause for the abrupt decrease in stress at that depth.

The difference plot on the top right of the figure shows a slight change in stress due to the 1m defect. A region of lower stress, shown in blue, can also be seen extending 0.3 m directly above the defect. A smaller region of higher stress can be seen below the defect, extending 0.1 m.

Figure 6.2 shows the fracture extent corresponding to the compression stress plot in Figure 6.1. The dry sand has a very weak bond with the concrete. The dry sand is separated from the concrete, to a depth of 1 m. The difference plots on the right show that the defect has no influence on cracking at this stage.

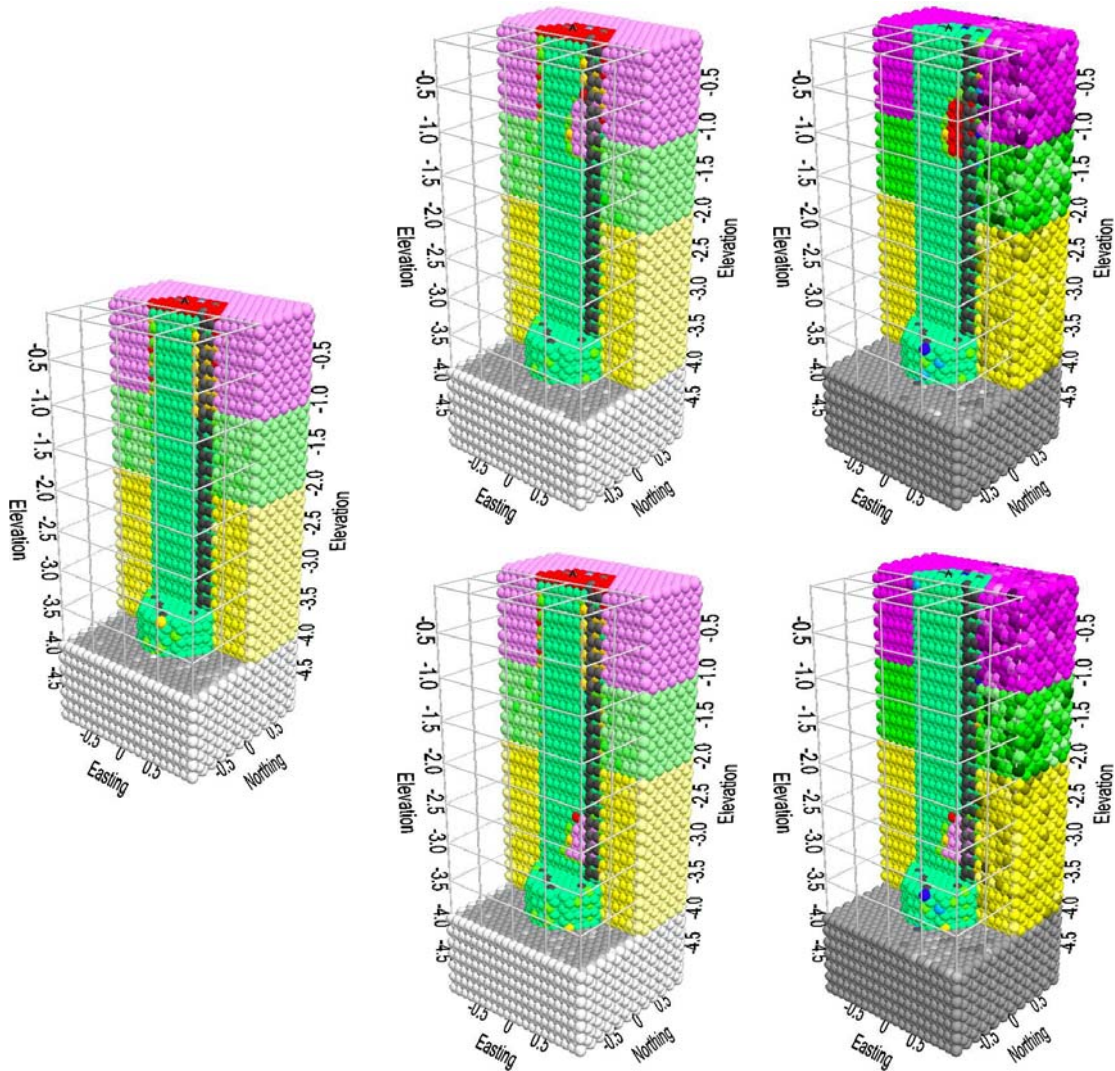


Figure 6.2. Plot. Fracture Extent at Initial Vertical Displacement. Top: Sand Intrusion at 1 m Depth. Bottom: Sand Intrusion 3 m Depth. Left: Fractures, No Defect. Center: Fractures. Right: Fracture Difference

The stress distribution in the surrounding soil is also of interest. The more the shaft settles, the more the sand and clay compact. This compaction strengthens the load bearing capacity of the ground, and ultimately of the shaft. The compaction also increases the friction and interlocking between the concrete and the ground, further improving shaft performance.

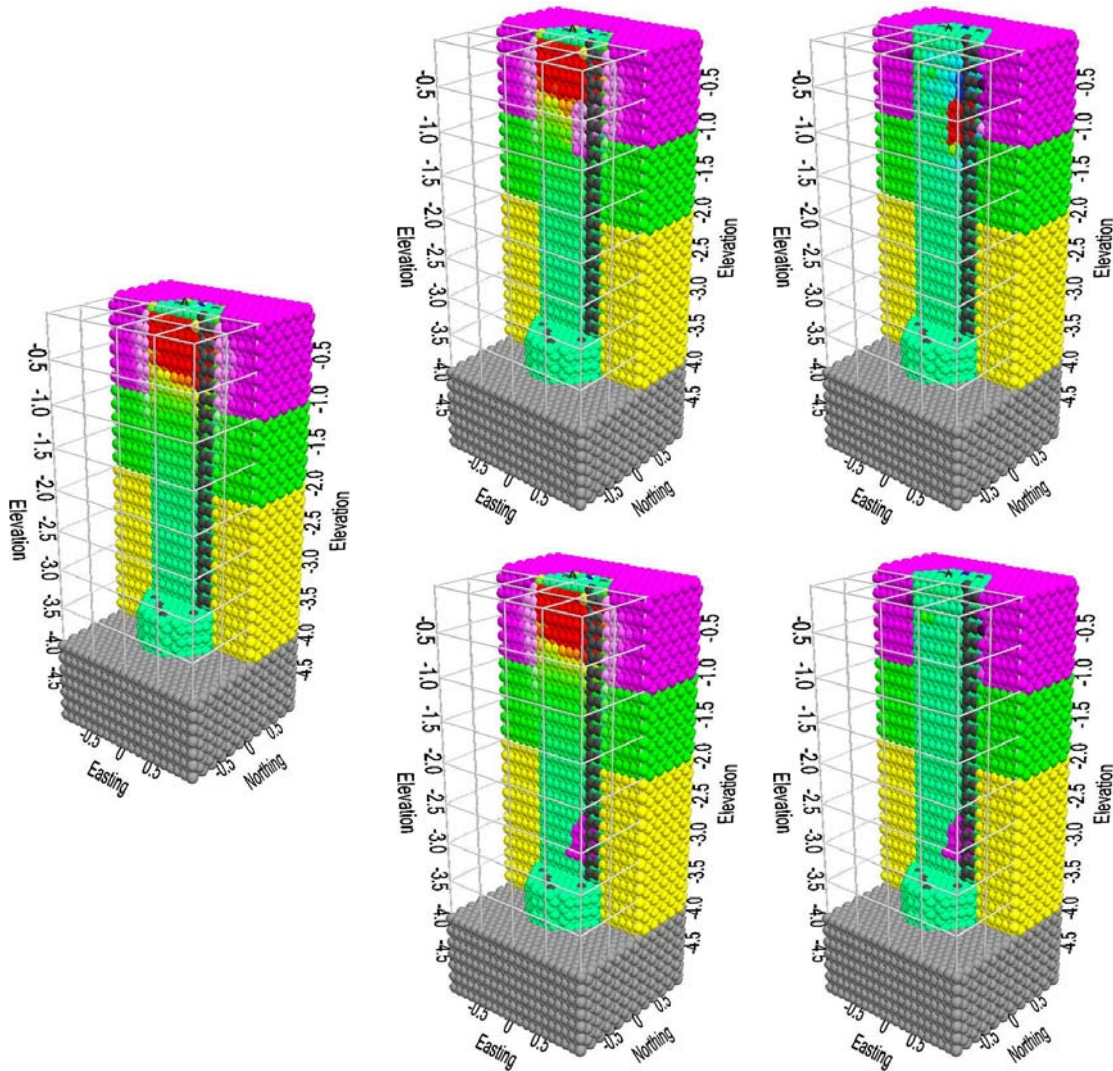


Figure 6.3. Plot. Compression Stress at 4 cm Vertical Displacement. Top: Sand Intrusion at 1 m Depth. Bottom: Sand Intrusion 3 m Depth. Left: Compression Stress, No Defect. Center: Compression Stress. Right: Compression Stress Difference

Figure 6.4 shows the fracture extent corresponding to the compression stress plot in Figure 6.3, at a displacement of 4 cm. At this stage, the concrete shows indications of significantly slipping away from the sand to a depth of 1.5 m, with separation forming between the concrete and clay to a depth of 3 m. Cracking can be seen to extend deeper in the right-most region of the shaft along the rebar. At this stage, the concrete is debonding from the rebar. On the other side of the shaft, at a region with no nearby rebar support, the concrete already shows signs of cracking at a depth of 0.5 m, indicated by a slightly lighter green color. The cracking is greatest at the outer left-hand region of the shaft, and gradually decreases to the center of the shaft. The difference plots on the right show that the defect still has no influence on cracking at this stage.

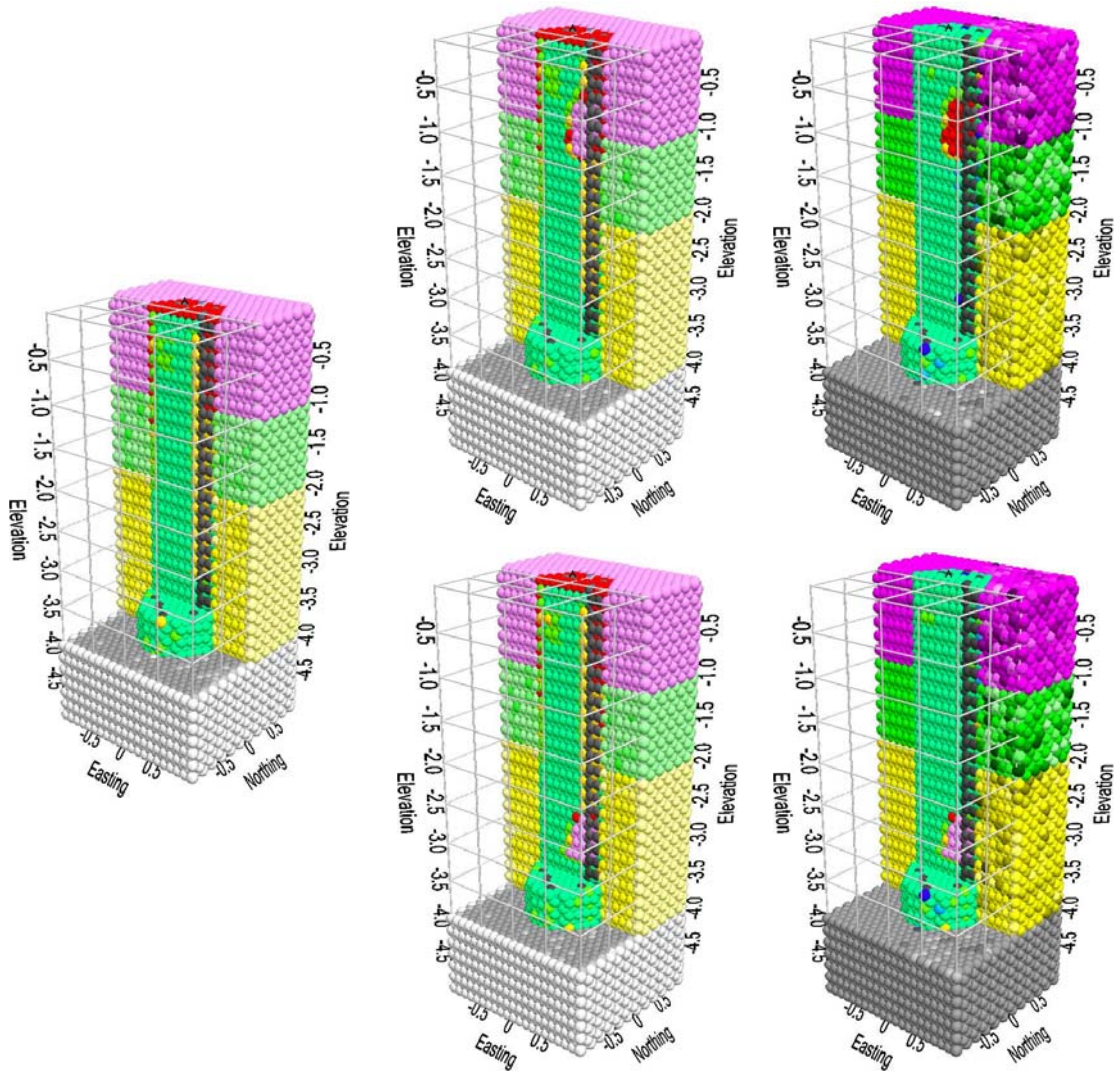


Figure 6.4. Plot. Fracture Extent at 4 cm Vertical Displacement. Top: Sand Intrusion at 1 m Depth. Bottom: Sand Intrusion 3 m Depth. Left: Fractures, No Defect. Center: Fractures. Right: Fracture Difference

6.1.3 Displacement of 8 cm

The stress intensity at a displacement of 8 cm is plotted in Figure 6.5. The shaft is now at peak load capacity. As seen from the plot on the left and the plots in the center, the compression stress is at very high levels in the top 1 m of the shaft. The stress abruptly decreases in the next 0.25 m, and gradually tapers off to nearly zero after a depth of 2.5 m. The shaft experiences the most compression between the surface down to 0.25 m below the top of the wet sand.

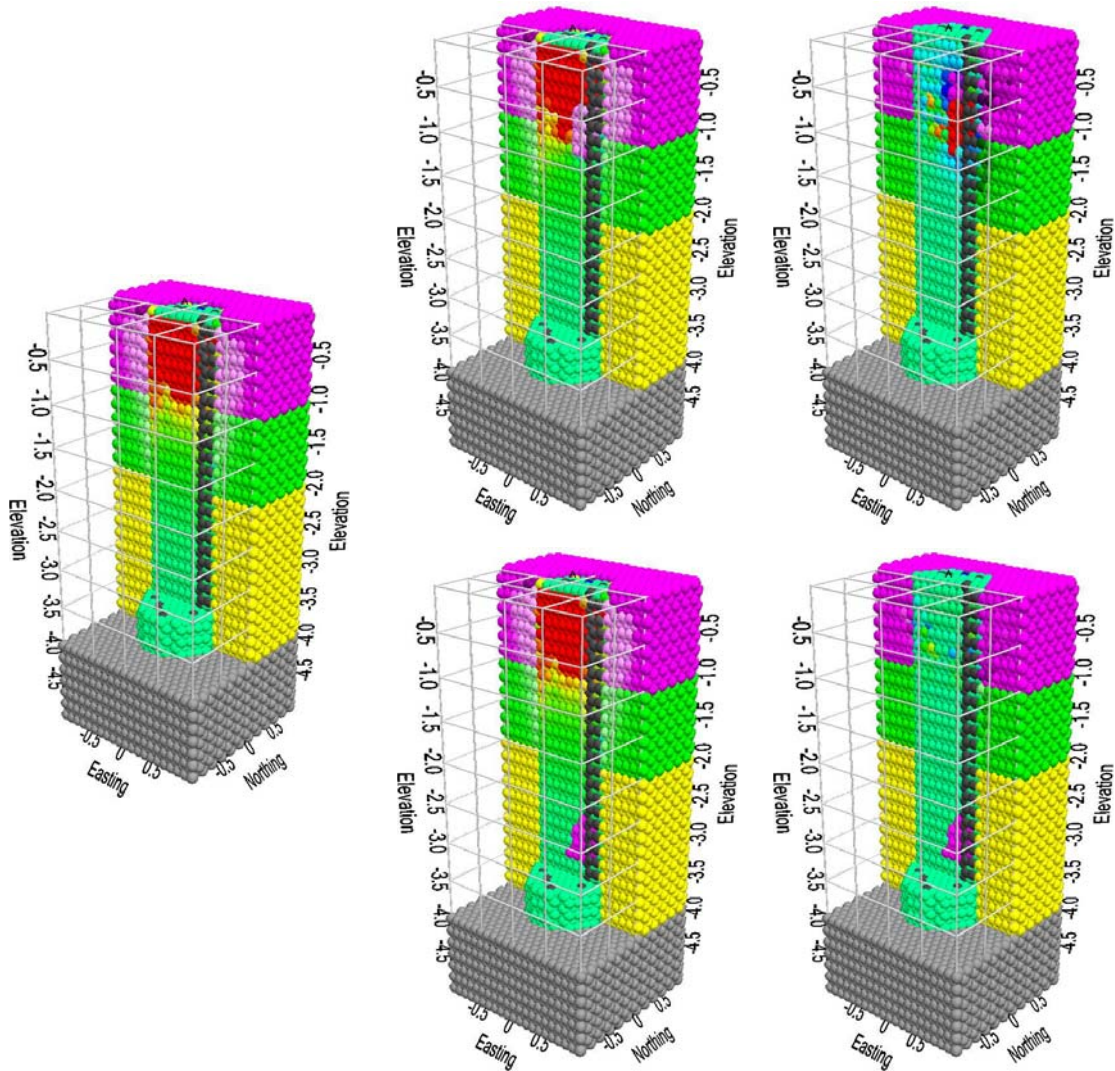


Figure 6.5. Plot. Compression Stress at 8 cm Vertical Displacement. Top: Sand Intrusion at 1 m Depth. Bottom: Sand Intrusion 3 m Depth. Left: Compression Stress, No Defect. Center: Compression Stress. Right: Compression Stress Difference

The difference plot in the top right of the figure shows a more significant change in stress due to the 1 m defect. The region of lower stress developing above the defect has both expanded in size and decreased in amplitude, shown in blue and purple. The smaller region of higher stress below the defect has significantly increased in amplitude to red, but a new region of lower stress has developed in a region extending 0.25 m below the higher stress region. There is also a small region of highly concentrated stress in the center of the shaft at a depth of 1 m shown in red, and another small region of highly concentrated stress slightly to the left of center at a depth of 0.75 m shown in orange. High concentrated stresses form as cracks develop and propagate, and these small regions of concentrated stress correspond to crack propagation, as shown in Figure 6.6.

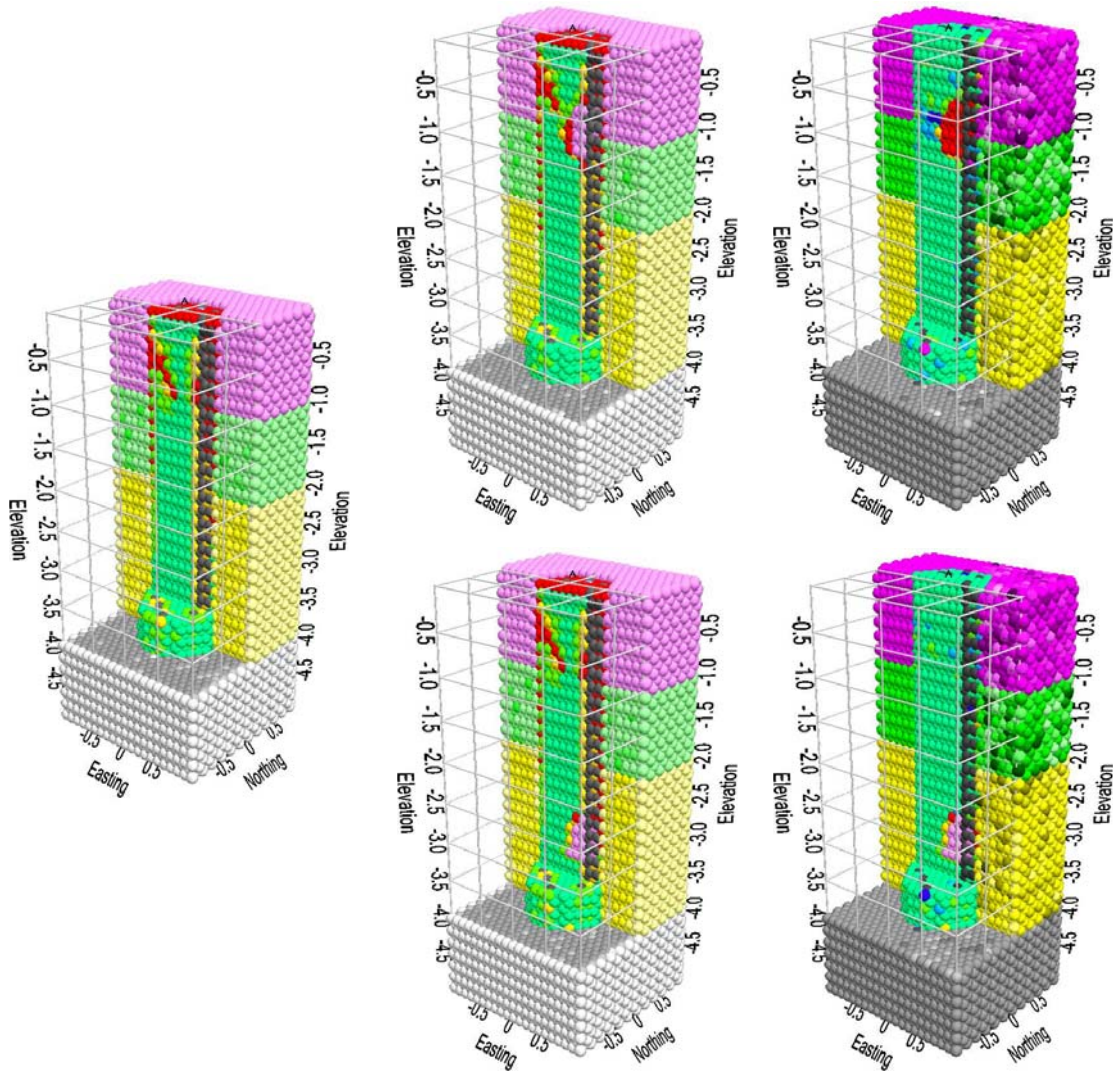


Figure 6.6. Plot. Fracture Extent at 8 cm Vertical Displacement. Top: Sand Intrusion at 1 m Depth. Bottom: Sand Intrusion 3 m Depth. Left: Fractures, No Defect. Center: Fractures. Right: Fracture Difference

Cracks release stress and change stress distribution. Therefore, cracks must be taken into account when attempting to understand stress behavior. The defect itself may at times acts as a large crack, redistributing stress and affecting crack propagation.

Figure 6.6 shows the fracture extent corresponding to the compression stress plot in Figure 6.5, at a displacement of 8 cm. At this stage, the concrete shows indications of significantly breaking away from the sand to a depth of 1.9 m in the shaft with no defect, 2.1 m in the shaft with the 3 m defect, and 2.25 m in the shaft with the 1 m defect. All three shafts show distinct crack development from the left side of the shaft at a depth of 0.25 m, extending to the center of the shaft at a depth of 1 m. However, the crack in the shaft with the 1 m defect appears to be at least 0.1 m shorter than the cracks in the other two shafts. This is a case of the defect altering crack

propagation. The small concentrated regions of high stress shown in the top right plot in Figure 6.5 indicate that two cracks are developing simultaneously in the shaft with the 1 m defect. One crack is propagating downward from the left side of the shaft, while another crack is propagating upward from the center of the defect. The crack from the defect changes the stress distribution, reducing the length of the downward propagating crack.

6.1.4 Displacement of 12 cm

The stress intensity at a displacement of 12 cm is plotted in Figure 6.7. The shaft is now considered to be in the plunging stage. As seen from the plot on the left and the plots in the center, the compression stress is at very high levels in the top 1.25 m of the shaft. The stress abruptly decreases, and will not significantly change with subsequent loading. At this point, the shaft has fully fractured, as shown in Figure 6.8, redistributing stress outward into the surrounding sand.

The difference plot in the top right of the figure shows an interesting change in stress due to the 1m defect. The region of lower stress still remains above the defect. However, the stress in the sand to the right of the shaft is significantly lower. This is not because the stress in the sand has decreased in the shaft with the 1 m defect, but because the stress in the sand has increased in the shaft with the 3 m defect and the shaft with no defect. This difference in stress is due to the difference in lateral displacement of the upper portion of the fractured concrete after shaft failure. The difference plot in the lower right of the figure shows a slight change in stress concentration along the fracture line. This indicates that the 3 m defect has an effect on stress in the region of the fracture, but not on the region at the surface. Therefore, the 3 m defect does not significantly affect load capacity in this scenario.

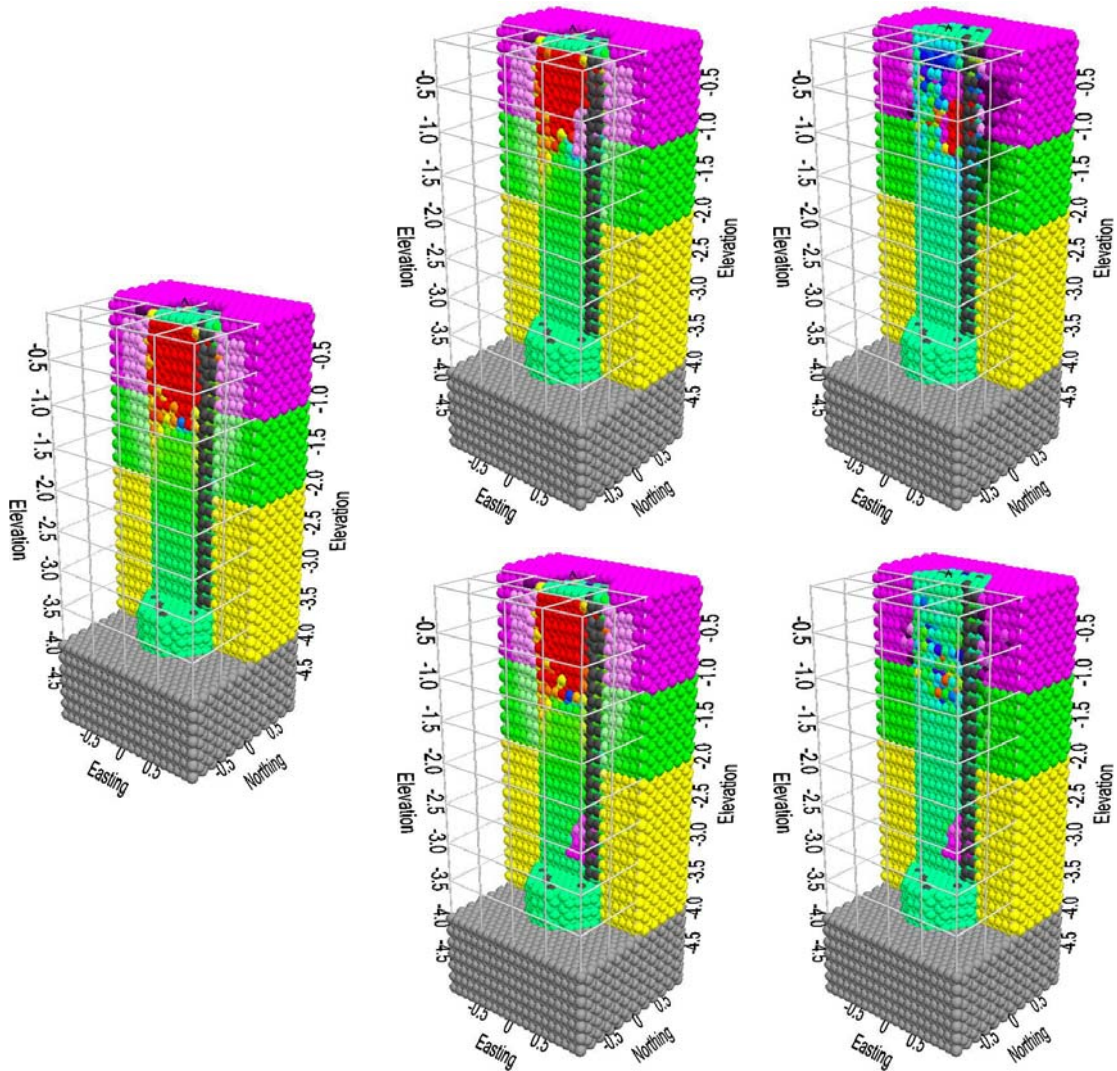


Figure 6.7. Plot. Compression Stress at 12 cm Vertical Displacement. Top: Sand Intrusion at 1 m Depth. Bottom: Sand Intrusion 3 m Depth. Left: Compression Stress, No Defect. Center: Compression Stress. Right: Compression Stress Difference

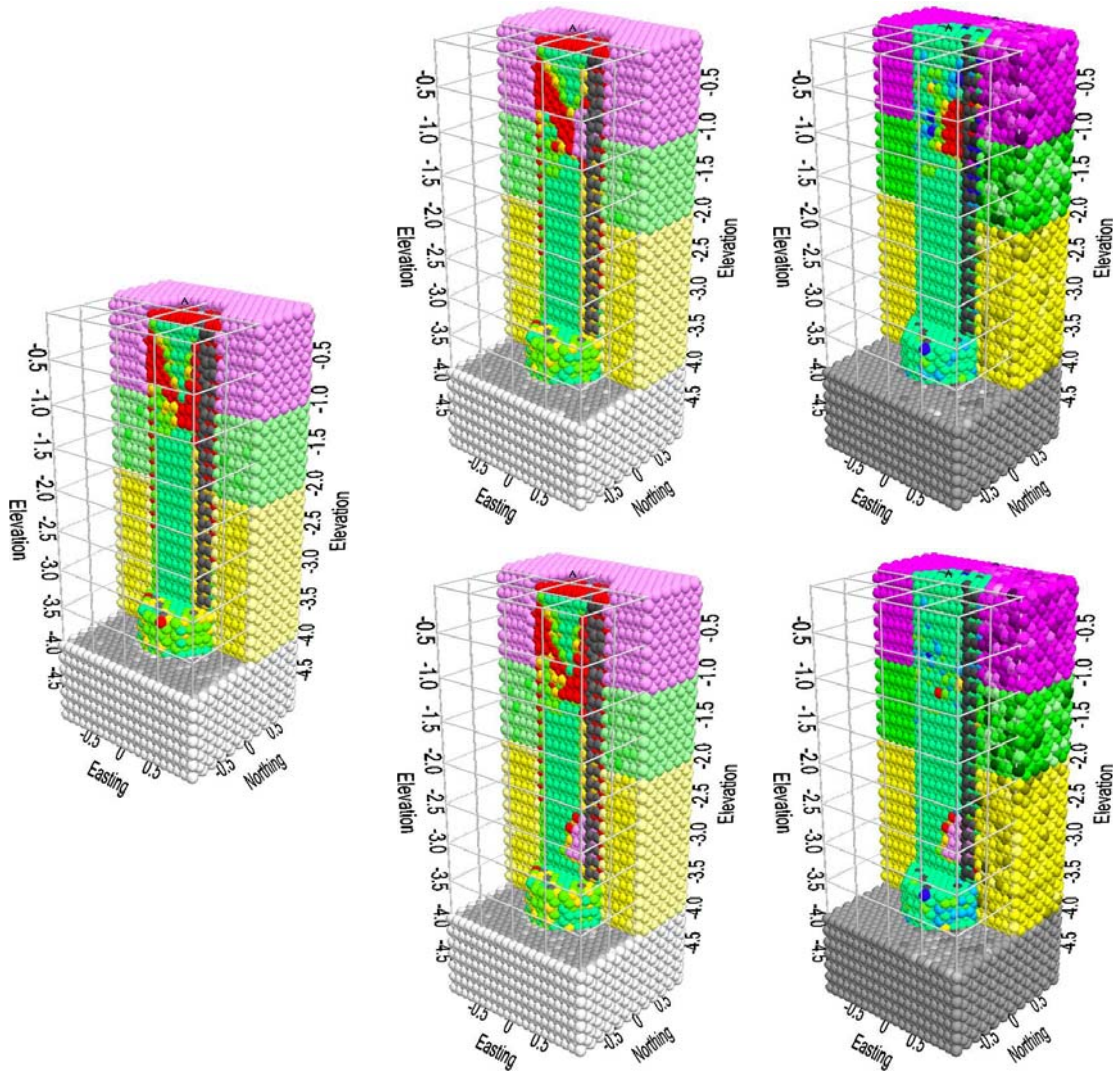


Figure 6.8. Plot. Fracture Extent at 12 cm Vertical Displacement. Top: Sand Intrusion at 1 m Depth. Bottom: Sand Intrusion 3 m Depth. Left: Fractures, No Defect. Center: Fractures. Right: Fracture Difference

6.1.5 Displacement of 16 cm and 20 cm

The stress intensity at a displacement of 16 cm is plotted in Figure 6.9. Figure 6.10 shows the fracture extent corresponding to the compression stress plot in Figure 6.9. The shaft is still considered to be in the plunging stage, after the load bearing capacity has stabilized. The upper portion of the shaft continues to bulge as it fails, and compress the surrounding sand.

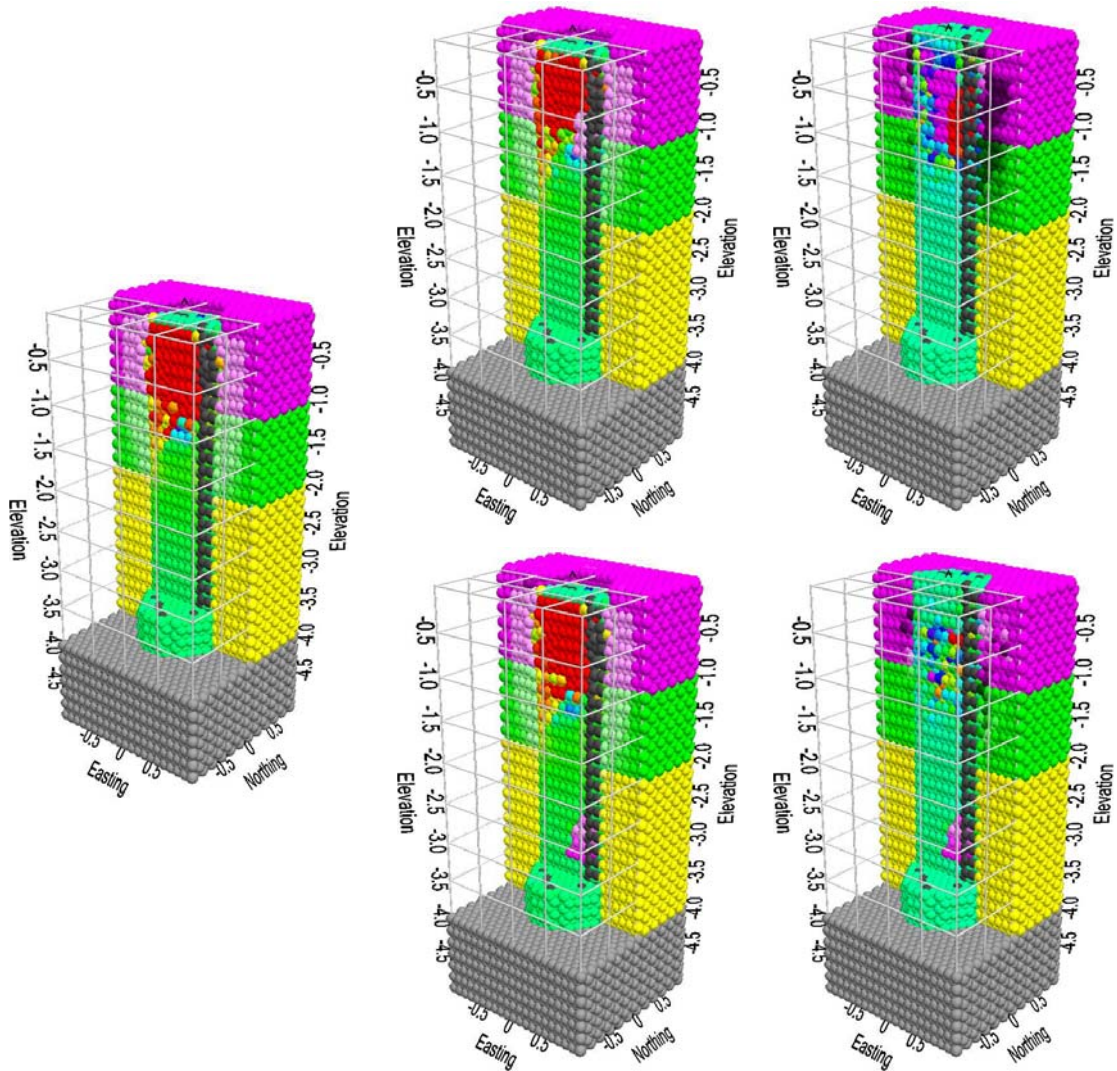


Figure 6.9. Plot. Compression Stress at 16 cm Vertical Displacement. Top: Sand Intrusion at 1 m Depth. Bottom: Sand Intrusion 3 m Depth. Left: Compression Stress, No Defect. Center: Compression Stress. Right: Compression Stress Difference

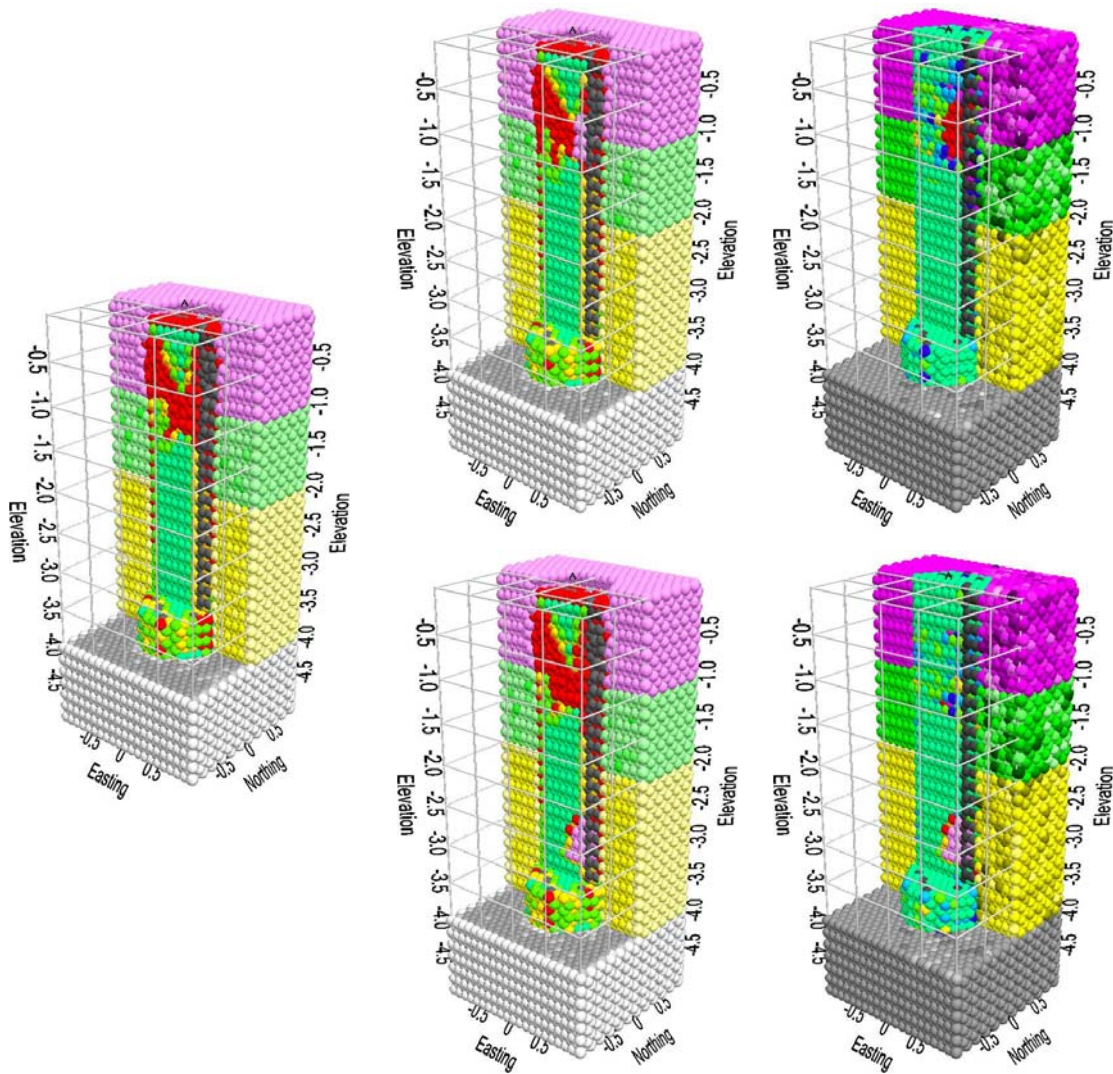


Figure 6.10. Plot. Fracture Extent at 16 cm Vertical Displacement. Top: Sand Intrusion at 1 m Depth. Bottom: Sand Intrusion 3 m Depth. Left: Fractures, No Defect. Center: Fractures. Right: Fracture Difference

The compression stress at a displacement of 20 cm is plotted in Figure 6.11. Figure 6.12 shows the fracture extent corresponding to the compression stress plot in Figure 6.11. The shaft is still considered to be in the plunging stage. The upper portion of the shaft continues to bulge as it fails, and compress the surrounding sand.

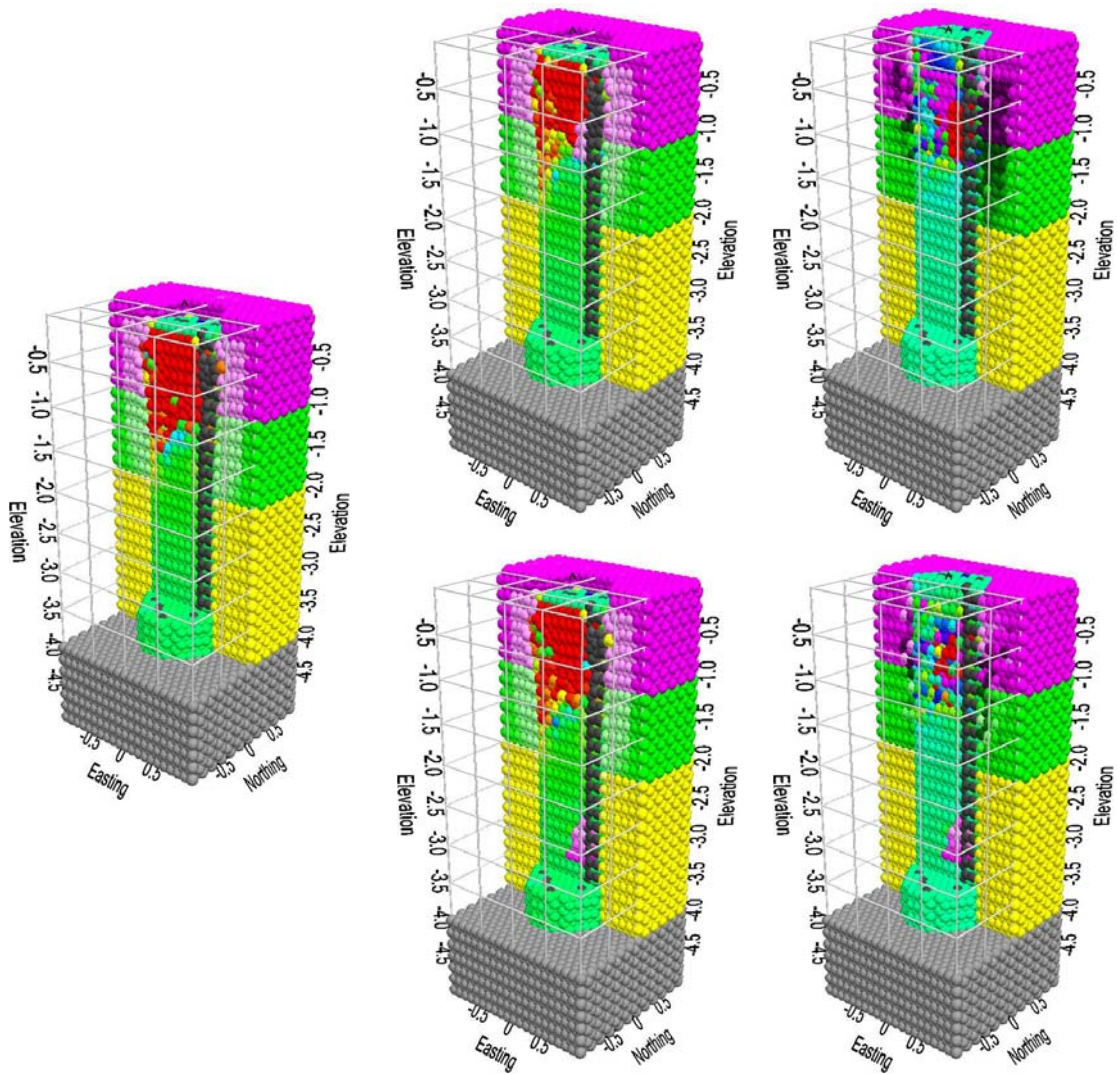


Figure 6.11. Plot. Compression Stress at 20 cm Vertical Displacement. Top: Sand Intrusion at 1 m Depth. Bottom: Sand Intrusion 3 m Depth. Left: Compression Stress, No Defect. Center: Compression Stress. Right: Compression Stress Difference

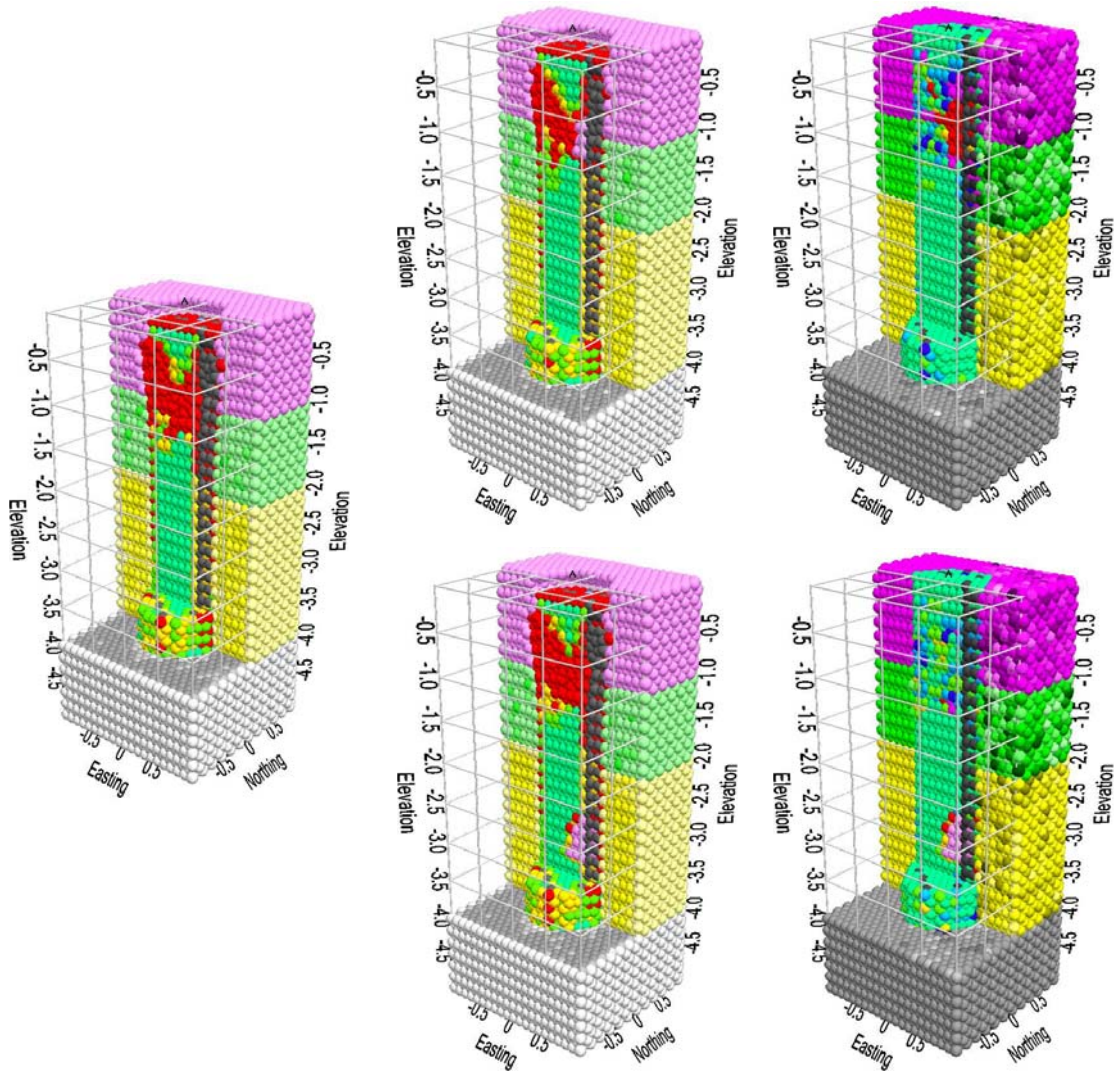


Figure 6.12. Plot. Fracture Extent at 20 cm Vertical Displacement. Top: Sand Intrusion at 1 m Depth. Bottom: Sand Intrusion 3 m Depth. Left: Fractures, No Defect. Center: Fractures. Right: Fracture Difference

6.2 Load-Settlement Curve Analysis

The load-settlement curves obtained from the numerical tests are shown in Figures 6.13 – 6.15. The figures clearly show the effects of the surrounding soil and rock. It is understood from both in situ and laboratory tests that the load-settlement curve undergoes a distinct “plunge” if the surrounding soil is soft clay, but no clear point of failure on the curve can be seen for the shaft in sands, intermediate soils, and stiff clays.

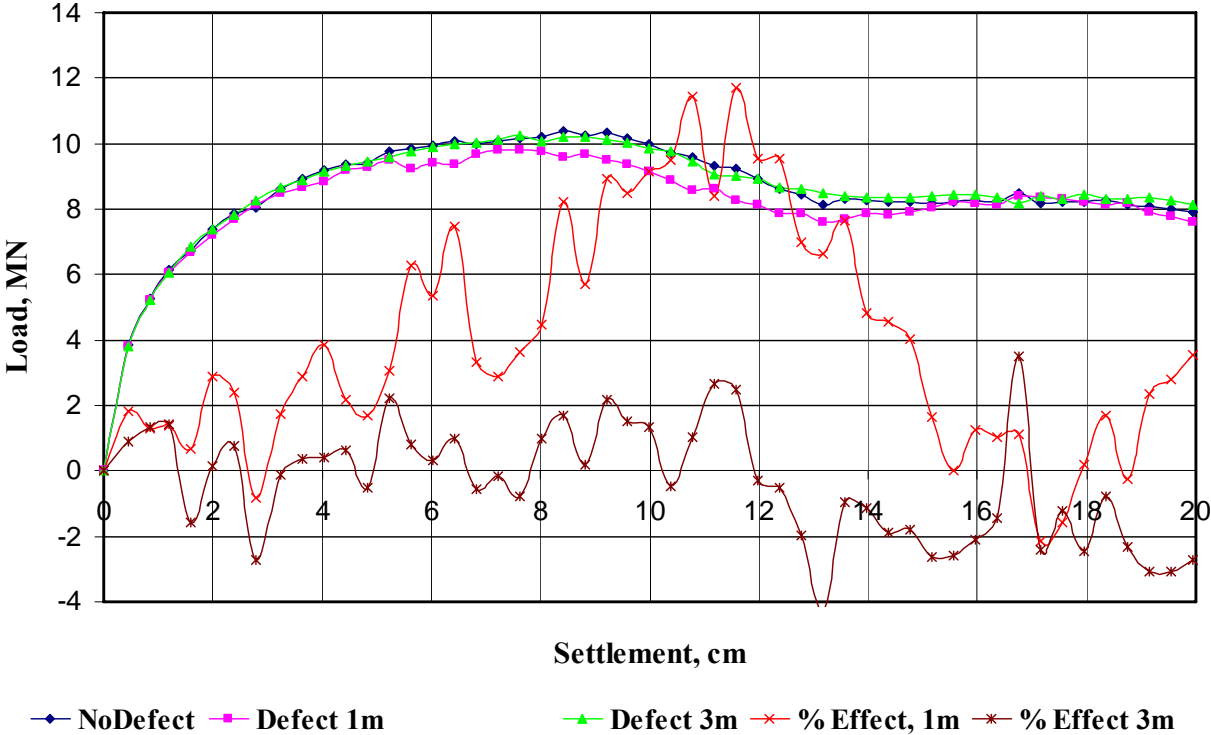


Figure 6.13. Chart. Effect of a Defect at Two Different Depths on Load Bearing Capacity

Many different methods have been proposed for interpreting this type of load-settlement curve without the plunge point. The Davisson’s method is commonly recommended in specifications and procedures that defines ultimate bearing capacity at a settlement of 4 mm as:

$$P_{ult} = 4 \text{ mm} + B/120 + PD/AE \tag{6.1}$$

where

- P_{ult} is ultimate capacity
- B is the foundation diameter
- P is applied load
- D is the foundation depth
- A is the foundation cross-sectional area
- E is the foundation elastic modulus

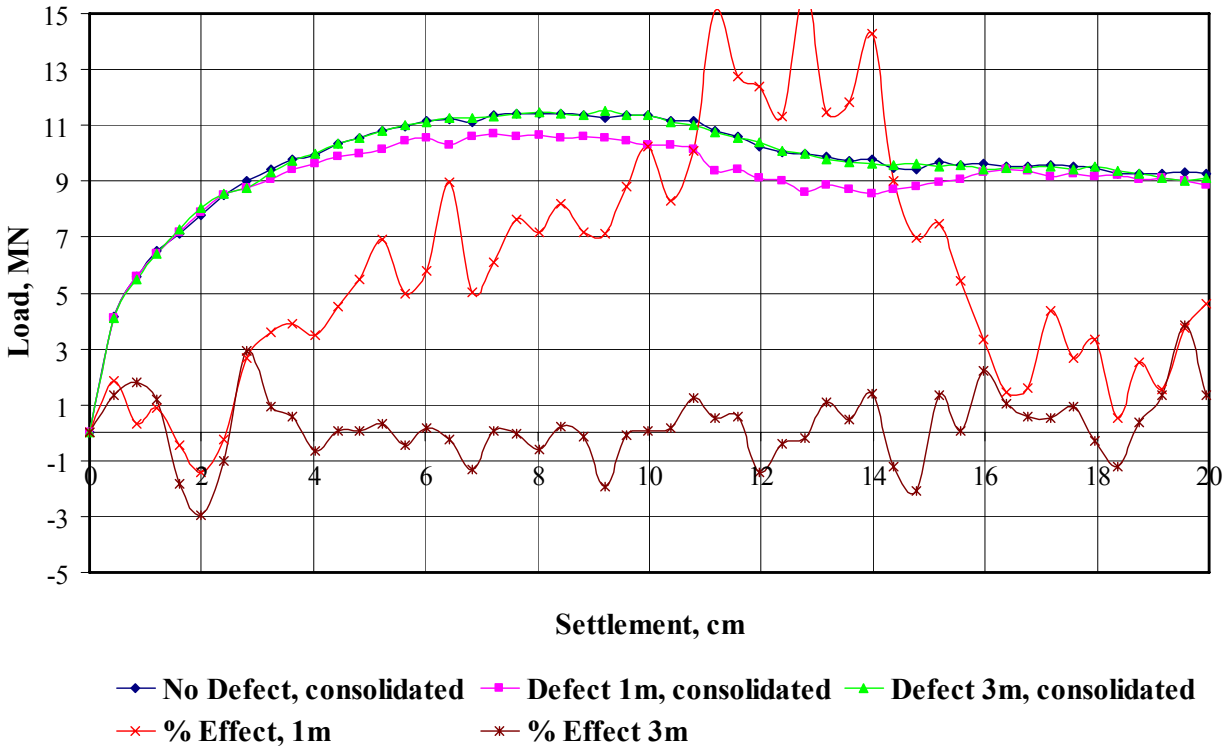


Figure 6.14. Chart. Effect of a Defect on Load Bearing Capacity with Shaft in Compacted Soil

6.2.1 Loosened Soil

Figure 6.13 is a graph of the loading curves from the axial load test performed in the previous section. The surrounding sand and clay were assumed to be loosened, a typical condition that occurs after soil is affected by excavation and thermal contraction after concrete curing. The load-settlement curves are typical of the ground conditions. The load initially increases sharply, then gradually peaks at about 8 cm displacement. The plunging phase begins at approximately 5 cm displacement.

The effect on load bearing capacity from the drilled shaft with the 1 m the 3 m defect is plotted as a percentage, compared with the shaft with no defect. The 3 m defect shows no significant change in shaft load capacity throughout the test. Although the difference in shafts load capacity for the 1 m defect exceeds 10%, this is at a displacement far beyond the failure criteria of 2.5 cm. There is actually no significant change in load performance for either defective shaft in the first 2.5 cm of displacement.

Figure 6.14 is a graph of the loading curves from an axial load test performed using the same shafts in the previous section, but with compacted sand and clay layers surrounding the drilled shaft. This condition could be produced by compacting the ground around the shaft near the surface, by pressurizing the concrete during placement, or by surrounding the shaft with a few

jet-grouted micro-piles or driven piles to compact the soil. Figure 6.14 is relatively equivalent to the test conducted with loosened soil, shown in Figure 6.13.

Figure 6.15 compares the loading curves from the two tests. The effect of soil compaction is far more significant than the effect of the defect. The improvement in load capacity in the first 2.5 cm reaches an average of nearly 10%. This suggests that the primary control factor is not the slight variations in concrete quality, but in the condition of the surrounding soil in the near surface.

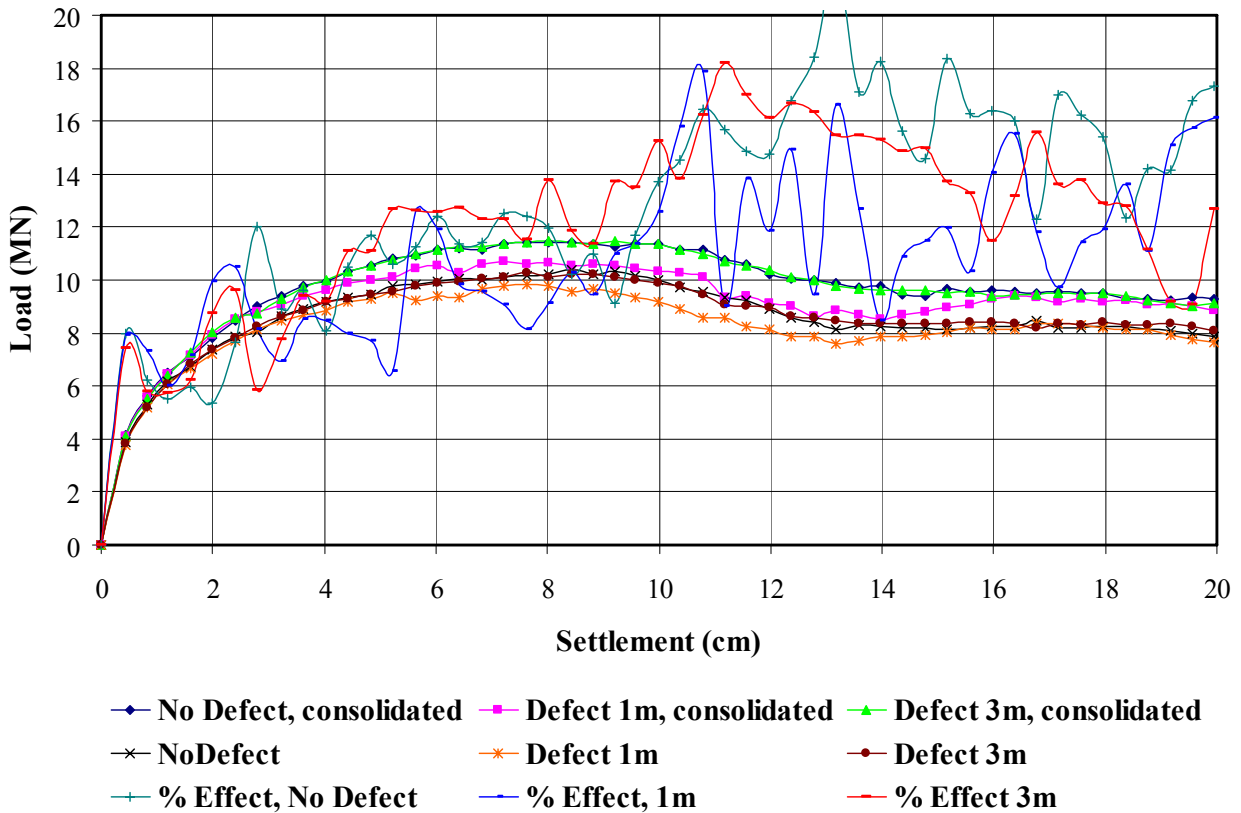


Figure 6.15. Chart. Effect of Soil Compaction on Load Bearing Capacity

6.3 Discussion

The modeling and analysis above show that the stress in the drilled shaft is not uniformly distributed through out the depth of the shaft. Soil density, friction angles of geo-materials, defects in the shaft, and compaction levels are the major control factors for stress concentration. In these stress concentration zones, local stresses may exceed the strength of the material to cause local failure within the material. In these stress concentration zones, materials may also experience large plastic deformations, which aggravate the propagation of cracks and worsen the corrosion process. Further stress analysis with fracture and non-elastic constitutive modeling in the stress concentration zones is recommended for further study.